Optimization of Sulfate Aerosol Hygroscopicity Parameter in WRF-Chem

Ah-Hyun Kim[1], Seong Soo Yum[1], Dong Yeong Chang[1], and Minsu Park[1]

[1]Department of Atmospheric Sciences, Yonsei University, Seoul, postal 03722, Korea

5   *Correspondence to*: Seong Soo Yum (ssyum@yonsei.ac.kr)

Abstract. A new sulfate aerosol hygroscopicity parameter (κ_{SO_4}) parameterization is suggested that is capable of considering the two major sulfate aerosols, H_2SO_4 and $(NH_4)_2SO_4$, using the molar ratio of ammonium to sulfate (R). An alternative κ_{SO_4} parameterization method is also suggested that utilizes typical geographical distribution patterns of sulfate and ammonium, which can be used when ammonium data is not available for model calculation. Using the Weather Research and Forecasting

10   coupled with Chemistry model (WRF-Chem), impacts of different κ_{SO_4} parameterizations on cloud microphysical properties and cloud radiative effects in East Asia are examined. Comparisons with the observational data obtained from an aircraft field campaign suggest that the new κ_{SO_4} parameterizations simulate more reliable aerosol and CCN concentrations, especially over the sea in East Asia than the original κ_{SO_4} parameterization in WRF-Chem that assumes sulfate aerosols as $(NH_4)_2SO_4$ only. With the new κ_{SO_4} parameterizations, the simulated cloud microphysical properties and precipitation became significantly

15   different, resulting in greater cloud albedo effect of about -1.5 W m^{-2} in East Asia than that with the original κ_{SO_4} parameterization. The new κ_{SO_4} parameterizations are simple and readily applicable to numerical studies of investigating the impact of sulfate aerosols in aerosol-cloud interactions without additional computational expenses.

1 Introduction

Aerosols impact global climate by directly scattering and absorbing radiation. Aerosols also play an important role

20   as potential cloud condensation nuclei (CCN). Increases in CCN number concentration could increase cloud optical depth, suppress local precipitation, and prolong cloud lifetime (Twomey, 1974; Albrecht, 1989). Therefore, the aerosol induced changes of cloud microphysical property can alter the Earth's radiation budget and hydrological cycle. Such aerosol-cloud interactions possibly cause the greatest uncertainty in the estimation of climate forcing due to their complexity (Myhre et al., 2013). Understanding the role of aerosols as CCN (CCN activation) is therefore important for predicting future climate. CCN

25   activation depends on the chemical and physical properties of aerosols (Köhler 1963; Abdul-Razzak et al., 1998; Dusek et al., 2006; Fountoukis and Nenes, 2005; Khvorostyanov and Curry, 2009; Ghan et al., 2011). Soluble aerosol species have high potential to become CCN and differences in aerosol solubility could exert a considerable impact on CCN activation (Nenes et al., 2002; Kristjánsson 2002).

Sulfate aerosols are one of the major components of natural and anthropogenic aerosols, contributing to a large

30   portion of the net radiative forcing due to aerosol-cloud interactions (Boucher et al, 2013). They are highly soluble and thereby

easily activated to become cloud droplets. Recently, Zelinka et al. (2014) estimated that the contribution of sulfate aerosols to the net effective radiative forcing from aerosol-cloud interaction (ERFaci) is about 64%. Sulfate aerosols are mainly present as sulfuric acid (H_2SO_4) and ammonium sulfate ((NH_4)$_2SO_4$) in the atmosphere (Charlson and Wigley, 1994), but have very different hygroscopicity parameter (κ) that represents the water affinity of aerosols and determines the efficiency of CCN

35 activation (Petters and Kreidenweis, 2007). Despite the importance of sulfate aerosols in the estimation of ERFaci, many atmospheric models treat sulfate aerosols simply assuming that they have a single κ_{SO_4} value (Ackermann et al., 1998; Stier et al. 2006; Pringle et al., 2010; Mann et al., 2011; Chang et al., 2017; Tegen et al., 2019).

Especially in East Asia, distribution of κ_{SO_4} value could vary significantly because the sulfur dioxide and ammonia are emitted from inland China on a massive scale (Kurokawa et al., 2013; Qu et al., 2016; Kang et al., 2016; Liu et al., 2017)

40 and the distribution of H_2SO_4 and (NH_4)$_2SO_4$ are closely related to the emissions and chemical reactions of sulfur dioxide and ammonia. Sulfur dioxide is oxidized to H_2SO_4 and then neutralized to form (NH_4)$_2SO_4$ by ammonia. Generally, sulfur dioxide is released from industries and from the sea surface, and ammonia is discharged from livestock and farmland. For this reason, the ratio of ammonium to sulfate is observed to decrease as the distance from the land increases (Fujita et al., 2000; Paulot et al., 2015; Kang et al., 2016; Liu et al., 2017). Thus, applying a single hygroscopicity parameter for all sulfate aerosols in

45 atmospheric models can lead to uncertainty in quantifying CCN activation, particularly in East Asia.

This study proposes a new κ_{SO_4} parameterization that aims at simultaneously considering the two major sulfate aerosols, i.e., (NH_4)$_2SO_4$ and H_2SO_4 in WRF-Chem (the Weather Research and Forecasting model coupled with chemistry model). First, we describe the calculation of κ for different size modes of aerosols and suggest a new parameterization of κ_{SO_4}. The performance of the new κ_{SO_4} parameterization in estimating the effects of aerosol-cloud interactions is examined for the

50 domain of East Asia. The model results are compared with the aircraft measurement data obtained during the Korea–US Air Quality campaign (KORUS-AQ, Al-Saadi et al., 2016). Finally, we address the effects of the new κ_{SO_4} parameterizations in simulating (or calculating) cloud microphysical properties and cloud radiative effects in East Asia.

2 Model description

2.1 The WRF-Chem model

55 The WRF-Chem version 3.8.1 is designed to predict mesoscale weather and atmospheric chemistry (Grell et al., 2005; Fast et al., 2006; Skamarock et al., 2008; Peckham et al., 2011). The aerosol size and mass distributions are calculated with the Modal Aerosol Dynamics Model for Europe (MADE; Ackermann et al., 1998) that includes three log-normal distributions for Aitken, accumulation, and coarse mode particles. MADE considers the new particle formation process of homogeneous nucleation in H_2SO_4 and H_2O system (Wexler et al., 1994; Kulmala et al., 1998). MADE treats inorganic chemistry systems

60 as the default option and organic chemistry systems as coupling options. Inorganic chemistry systems include the chemical reactions of three inorganic ionic species, i.e. SO_4^{-2}, NO_3^- and NH_3^+ (Ackermann et al., 1998). The secondary organic aerosol

model (SORGAM), an optional model to calculate secondary organic aerosol (SOA) chemistry processes (Schell et al., 2001), is coupled to MADE (MADE/SORGAM). MADE/SORGAM treats atmospheric aerosols as an internal mixture of sulfate, nitrate, ammonium, organic carbon (OC), elemental carbon (EC), sea salt, and dust aerosols. Additionally, gas phase chemical processes are calculated in Regional Acid Deposition Mechanism version 2 (RADM2, Chang et al., 1989). RADM2 simulates the concentrations of air pollutants, including inorganic (14 stable, 4 reactive and 3 abundant stable) and organic (26 stable and 16 peroxy radicals) chemical species.

For the microphysics calculation, we use the CCN activation parameterizations (Abdul-Razzak and Ghan, 2000, hereafter ARG) and Morrison double-moment microphysics scheme (Morrison et al., 2009). The CCN activation is determined by meteorological factors (e.g., updraft) and physicochemical properties of aerosols based on the assumption of internally well-mixed aerosols. A detailed model designs for the modelling studies of aerosol–cloud interactions in WRF-Chem can be found in Gustafson et al. (2007), Chapman et al. (2009), Grell et al. (2011), and Baró et al. (2015).

For the physics parameterization, we use the following configurations: Rapid and accurate Radiative Transfer Model for GCMs (RRTMG) for the shortwave and longwave radiative transport processes (Iacono et al., 2008); Yonsei University scheme (YSU scheme) for the atmospheric boundary layer processes (Hong et al., 2006) ; the Unified NOAH (NCEP Oregon State University, Air Force, and Hydrologic Research Lab's) Land Surface Model for land surface processes (Tewari et al., 2004).

2.2 Calculation of the hygroscopicity parameter

The CCN activation parameterization is based on the Köhler theory that is described with the water activity and the surface tension of the solution droplets. The water activity is estimated from detailed information of aerosols such as Van't Hoff factor, osmotic coefficient, molecular weight, mass, and density of aerosols. If aerosol chemical information is fully provided, CCN activation could be almost accurately calculated using the Köhler theory (Raymond and Pandis, 2003). However, it requires high computational expenses (Lewis, 2008). Petters and Kreidenweis (2007) proposed a single quantitative measure of aerosol hygroscopicity, known as hygroscopicity parameter (κ). This method does not require detailed information of aerosol chemistry and thereby reduces computational cost when calculating the water activity. For this reason, κ values are applied in many observational, experimental, and numerical studies (Zhao et al., 2015; Shiraiwa et al., 2017; Chang et al., 2017; Gasteiger et al., 2018). κ can be determined separately for the three log-normal modes (Aitken, accumulation, and coarse modes). That is, κ_i is the volume-weighted average of κ_j for mode i:

$$\kappa_i \equiv \sum_{j=1}^{J} \varepsilon_{ij} \kappa_j, \tag{1}$$

where ε_{ij} is the volume ratio of chemical j in mode i (=$V_{ij}/V_{tot,i}$, $V_{tot,i} = \sum_{j=1}^{J} V_{ij}$, and V_{ij} is the volume of chemical j in mode i) and κ_j is the individual hygroscopicity parameter for chemical j. Eq. (1) is calculated with the assumption of the temperature, 298.15 K. The upper end of the κ value for hygroscopic species of atmospheric relevance is around 1.40 (Petter and Kreidenweis, 2007).

2.3 Limitation of previous κ_{SO_4} parameterizations

95   CCN activation is affected by κ values (e.g., Nenes et al., 2002; Kristjánsson 2002). H_2SO_4 has more than two times higher κ value than $(NH_4)_2SO_4$, i.e., 1.19 for $\kappa_{H_2SO_4}$ and 0.53 for $\kappa_{(NH_4)_2SO_4}$ (Clegg and Wexler, 1998; Petters and Kredenweis 2007; Good et al., 2010). Such large disparities of κ_{SO_4} between different sulfate species could cause a large variability in the estimation of ERFaci. However, many aerosol modules simplify the physical and chemical characteristics of aerosols, and often neglect some chemical species (Kukkonen et al., 2012; Im et al., 2015; Bessagnet et al., 2016). Sulfate aerosols are

100   usually prescribed as a single species of either H_2SO_4 or $(NH_4)_2SO_4$. Some models consider H_2SO_4 as the representative sulfate aerosol when the neutralization reaction between H_2SO_4 and ammonia is not considered or when only the binary sulfuric acid–water nucleation is considered (e.g., Mann et al., 2011; Kulmala et al., 1998; Korhonen et al., 2008; Stier et al., 2006; Wexler et al., 1994; Kazil and Lovejoy 2007). Some other models consider $(NH_4)_2SO_4$ as the representative sulfate aerosol when studying aerosol-CCN closure (e.g., VanReken et al., 2003) or when including the ternary sulfuric acid–ammonia–water

105   nucleation process or the neutralization reaction between sulfate and ammonia (Kulmala et al., 2002; Napari et al., 2002; Elleman and Covert, 2009; Watanabe et al., 2010; Grell et al., 2005). To reduce the uncertainty of ERFaci, more speciated κ_{SO_4} parameters need to be utilized in the calculation of cloud droplet activation process, at least, for the two main sulfate aerosols i.e., H_2SO_4 and $(NH_4)_2SO_4$. Here, we suggest a new method of representing κ_{SO_4} that considers both H_2SO_4 and $(NH_4)_2SO_4$ using the molar ratio of NH_4^+ to SO_4^{2-}. We also suggest an alternative method that utilizes the spatial distribution

110   of κ_{SO_4}, based on the distinct distribution patterns of NH_4^+ and SO_4^{2-} over land and sea.

2.4 New parameterization of κ_{SO_4}

         H_2SO_4 is completely neutralized as $(NH_4)_2SO_4$ when ammonia is abundant (Seinfeld and Pandis, 2006). During the neutralization process of H_2SO_4, one mole of SO_4^{2-} takes up two moles of NH_4^+ and forms one mole of $(NH_4)_2SO_4$. Here, the assumption is that ammonia neutralizes SO_4^{2-} ions prior to nitrate ions (Seinfeld and Pandis, 2006) and sulfate aerosols appear

115   only in the form of H_2SO_4 and $(NH_4)_2SO_4$. In the calculation of κ_{SO_4}, the proportion of H_2SO_4 and $(NH_4)_2SO_4$ is determined using the ammonium to sulfate molar ratio R $(=n_{NH_4^+}/n_{SO_4^{2-}}$, $n_{NH_4^+}$ is the molar concentration of NH_4^+ ions and $n_{SO_4^{2-}}$ is the molar concentration of SO_4^{2-} ions). Generally, sulfate aerosols are completely neutralized as $(NH_4)_2SO_4$ at high R conditions $(R>2)$, and partially neutralized at low R conditions $(R<2)$ (Waggoner et al., 1983; Fisher et al., 2011). Using R and the Zdanovskii–Stokes–Robinson relationship (i.e., $V_d = V_w + V_{tot}$, $V_{tot} = \sum_{j=1}^{J} V_j$, where V_d is the droplet volume, V_w is the

120   volume of water, and V_j is the volume of the chemical j), a representative κ_{SO_4} is defined as:

$$\kappa_{SO_4} = \varepsilon_{H_2SO_4}\kappa_{H_2SO_4} + \varepsilon_{(NH_4)_2SO_4}\kappa_{(NH_4)_2SO_4}, \tag{2}$$

where $\varepsilon_{H_2SO_4}$ is the volume fraction of H_2SO_4 in the total volume of sulfate aerosols ($=V_{H_2SO_4}/V_{SO_4}$; $V_{H_2SO_4}$ is the volume concentration of H_2SO_4, V_{SO_4} is the total volume concentration of sulfate aerosols), and $\varepsilon_{(NH_4)_2SO_4}$ is calculated likewise for $(NH_4)_2SO_4$ [$=V_{(NH_4)_2SO_4}/V_{SO_4}$; $V_{(NH_4)_2SO_4}$ is the volume concentration of $(NH_4)_2SO_4$]. In this study, we use 1.19 and 0.53 to represent $\kappa_{H_2SO_4}$ and $\kappa_{(NH_4)_2SO_4}$, respectively (Clegg and Wexler, 1998; Petters and Kredenweis 2007; Good et al., 2010). The volume fractions of H_2SO_4 and $(NH_4)_2SO_4$ are calculated as:

i)   if $R = 0$, then, $\varepsilon_{H_2SO_4} = 1$ and $\varepsilon_{(NH_4)_2SO_4} = 0$,

ii)   if $0 < R < 2$, then,

$$\varepsilon_{H_2SO_4} = \frac{\left[\left(1-\frac{R}{2}\right) \times n_{SO_4^{2-}}\right] \times \frac{m_{H_2SO_4}}{\rho_{H_2SO_4}}}{V_{SO4}} \text{ and } \varepsilon_{(NH_4)_2SO_4} = \frac{\left(\frac{R}{2} \times n_{SO_4^{2-}}\right) \times \frac{m_{(NH_4)_2SO_4}}{\rho_{(NH_4)_2SO_4}}}{V_{SO4}}, \tag{3}$$

iii)   if $R > 2$, then, $\varepsilon_{H_2SO_4} = 0$ and $\varepsilon_{(NH_4)_2SO_4} = 1$,

where m and ρ indicate the molar mass and density of the specific chemical species, respectively. To be more realistic, ammonium bisulfate may also need to be considered: when the number of SO_4^{2-} is smaller than NH_4^+, the sulfates appear as a mixture of ammonium bisulfates and sulfuric acids, and when the number of SO_4^{2-} is greater than NH_4^+ but not twice as large as NH_4^+, the sulfates appear as a mixture of ammonium bisulfates and ammonium sulfates (Nenes et al., 1998; Moore et al., 2011, 2012). For simplicity, however, such partitioning is not considered in this study. As a result, sulfate aerosols are treated as $(NH_4)_2SO_4$ when R is greater than two ($R>2$) and as H_2SO_4 when R is zero ($R=0$). This method is applicable to the models that considers both NH_4^+ and SO_4^{2-} ions. If NH_4^+ data is not available in a model, we suggest an alternative method to represent κ_{SO_4}, based on the typical geographical distribution pattern of sulfate aerosols available from observations as discussed below.

      Observational studies show the distinctly different distribution patterns of the two dominant sulfate aerosol species, i.e., $(NH_4)_2SO_4$ over land and H_2SO_4 over sea (Fujita et al., 2000; Paulot et al., 2015; Kang et al., 2016; Liu et al., 2017). Such distribution pattern is related to the sources of sulfate and ammonium. In general, sulfate aerosols are emitted from land and sea, while ammonium is mostly produced from lands. Sulfur dioxide is produced from fossil fuel combustions, volcanic eruptions and dimethyl-sulfide (DMS) via air-sea exchanges, and then forms sulfate aerosols (Aneja 1990; Jardin et al., 2015). Wind transportations of pollutants could also cause high concentration of sulfate aerosols over the sea (Liu et al., 2008). On the other hand, ammonium is emitted from livestock, fertilizer, and vehicles (Sutton et al., 2013; Paulot et al., 2014; Bishop et al., 2015; Liu et al., 2015; Stritzke et al., 2015), and therefore is concentrated mostly on lands. Ammonium is usually not abundant enough to fully neutralize H_2SO_4 in the marine boundary layer (Paulot et al., 2015; Ceburnis et al., 2016). Therefore, when the ammonium information is not available, the κ_{SO_4} can be alternatively estimated with the consideration of the land and sea fractions as:

$$\kappa_{SO_4} = f \times \kappa_{SO_4,land} + (1-f) \times \kappa_{SO_4,sea}, \tag{4}$$

where f represents the fraction of land at each grid point; unity means entire land, and zero means entire sea, and the value in-between represents the fraction of land at the grid points in the coastal areas. $\kappa_{SO_4,land}$ and $\kappa_{SO_4,sea}$ represent κ_{SO_4} over land and sea, respectively (i.e., $\kappa_{SO_4,land} = \kappa_{(NH_4)_2SO_4} = 0.53$ and $\kappa_{SO_4,sea} = \kappa_{H_2SO_4} = 1.19$).

3 Experimental setup

150   Model simulations are carried out for thirty-six days from 0000 UTC 10 May to 0000 UTC 15 June 2016 and the first five days are used as a spin-up time. Observational data for sulfate aerosols and CCN during this period were obtained from the KORUS-AQ campaign and they indicated that sulfate aerosols were widely distributed throughout East Asia due to the stagnation of high-pressure systems and the transportation of pollutants from China. The domain covers East Asia (i.e., 2,700 km × 2,700 km; 20°N–50°N, 105°E–135°E) with 18 km grid spacing and 50 vertical levels from the sea level pressure to 100

155   hPa. The initial and boundary conditions are provided by the National Center for Environment Prediction–Climate Forecast System Reanalysis (NCEP–CFSR) (Saha et al., 2014). The 4DDA (4 Dimensional Data Assimilation) analysis nudging is used. Anthropogenic emission inventories are obtained from Emissions Database for Global Atmospheric Research–Hemispheric Transport of Air Pollution (EDGAR–HTAP; Janssens-Maenhout et al., 2015). Natural source emission inventories adopt the Model of Emissions of Gases and Aerosols from Nature (MEGAN; Guenther et al., 2006).

160   We conduct four simulations with different κ_{SO_4} parameterizations: 1) AS uses a single κ_{SO_4} of 0.53 (i.e., $\kappa_{(NH_4)_2SO_4}$), assuming that all sulfate aerosols are completely neutralized by ammonium, which is a default setting in WRF-Chem; 2) SA uses a single κ_{SO_4} of 1.19 (i.e., $\kappa_{H_2SO_4}$) assuming that all sulfate aerosols are H$_2$SO$_4$; 3) RA applies the new κ_{SO_4} parameterization that calculates the volume weighted mean κ_{SO_4} by using the molar ratio of ammonium to sulfate (R) (i.e., eq. 2); and 4) LO adopts different κ_{SO_4} for land and sea, assuming that sulfate aerosols are completely neutralized as (NH$_4$)$_2$SO$_4$

165   over land and are H$_2$SO$_4$ only over sea (i.e., eq. 4).

4 Results and discussions

4.1 Distribution of sulfate and ammonium

The simulated sulfate and ammonium distributions are compared with the observational data measured onboard the NASA DC-8 aircraft during the KORUS–AQ campaign (https://www-air.larc.nasa.gov/missions/korus-aq/), in and around the Korean

170   Peninsula in May and June of 2016. The measurements are taken within the boundary layer. The mass concentration of sulfate and ammonium were obtained by the method described in Dibb et al. (2003).

    In Fig. 1, the mass concentration of sulfate and ammonium simulated by AS are compared with the KORUS-AQ aircraft observations (OBS) following the flight track. The simulated sulfate shows a positive bias but has a high temporal correlation with OBS (r=0.78). The simulated ammonium is less biased than sulfate but indicates a moderate temporal

175   correlation with OBS (r=0.58). Overall, it seems reasonable to state that the WRF-Chem model can calculate the distribution of sulfate aerosols well enough.

Fig. 2 shows 30 days averaged mass concentration of sulfate and ammonium and the molar ratio (R) of ammonium to sulfate over the model domain. During the KORUS-AQ campaign period, high-pressure systems often covered East China and the Yellow Sea and that led to stagnating sulfate and ammonium concentrations. However, sulfate and ammonium are distributed differently due to different sources. Pollutants emitted from the Asian continent are often transported by westerly and southerly winds. Sulfate is highly concentrated in China and the northern part of the Yellow Sea, and DMS emission from the sea also contributes to the formation of sulfate aerosols over the sea. Ammonium is widely distributed throughout China due to the use of fertilizers over farmlands (Van Damme et al., 2014; Paulot et al., 2014; Warner et al., 2017). The concentration of ammonium is generally low over the sea, but over the northern part of the Yellow Sea it is high due to wind transport.

The distribution of R is associated with the distribution of sulfate and ammonium (Fig. 2). In general, R is high ($R>2$) over the land on account of the high anthropogenic emissions of continental ammonium, and R is low ($R<2$) over the remote seas because the ammonium concentration is small. However, high R is also shown over the Yellow Sea in Fig. 2. This is because the ammonium concentration increases when the westerlies carry continental pollutants over the Yellow Sea during the simulation period. Based on the distribution of R, sulfate aerosols are expected to be almost completely neutralized over land [e.g., $(NH_4)_2SO_4$] and partially neutralized over sea [$(NH_4)_2SO_4+H_2SO_4$].

4.2 Distribution of κ

Fig. 3 shows the average κ of the accumulation mode aerosols in AS and the difference between RA and AS, and LO and AS. The accumulation mode is selected because sulfate aerosols are dominant in this mode. AS simulates κ values that are roughly consistent with the observed mean κ values in the literature (i.e. κ over land is about 0.3 and κ over sea is about 0.7; Andreas and Rosenfeld, 2008), but it varies significantly between land and sea. The κ over land is expected to be lower than the κ over sea because continental aerosols usually include more hydrophobic aerosol species such as black carbon and organic carbon from industries, while maritime aerosols consist mainly of hygroscopic substances, i.e. sea salt and non-sea salt sulfates originated from DMS. The variation of κ is also influenced by chemical reactions and meteorological factors, i.e. wind transportations of aerosols and scavenging of aerosols due to precipitations, as well as gravitational settling.

Compared to AS, RA and LO show pronounced difference of κ over sea (Figs. 3b and 3c). That is, RA and LO produce significantly higher κ over the sea than AS does because ammonium concentration is not sufficient enough to neutralize sulfate completely over the sea (i.e. R<2). RA predicts slightly higher continental κ following the coastal regions than AS because R becomes occasionally low due to the intrusion of maritime air mass that has very low concentration of ammonium. Maritime κ of RA is lower than that of LO because the transportation of continental pollutants increases the portion of ammonium over the Yellow sea.

4.3 CCN activation

According to the Köhler theory, changes in κ directly influence CCN activation. In this study, the CCN activation rate (f_{CCN}) is defined as the ratio of the CCN number concentration at 0.6% supersaturation to the total aerosol number

concentration. Simulated f_{CCN} is compared with the aircraft measurements during the KORUS-AQ campaign (OBS). During
this campaign, aerosol and CCN number concentrations were measured by a condensation particle counter (CPC; TSI 3010)
and a CCN counter (CCNC; DMT CCN-100), respectively (Park et al., 2020). The CPC measures the number concentration
of aerosols larger than 10 nm in diameter, and the CCNC measures the CCN number concentration at 0.6% supersaturation.

The model simulations well capture the temporal variation of f_{CCN} (r~0.7 for the linear correlation with OBS; Fig.
4). However, f_{CCN} are underestimated mainly due to the underestimation of CCN concentrations. The average aerosol (CN)
number concentrations for the flight track in all simulations (AS, SA, RA, and LO) and the actual observed values during the
flight are 5934 cm^{-3} and 5794 cm^{-3}, respectively. So unlike Georgiou et al. (2018) that showed that the WRF-Chem coupled
with MADE/SORGAM tended to overestimate aerosol number concentrations, our simulations only slightly overestimated
aerosol number concentrations. The average CCN number concentration at 0.6% supersaturation for AS, RA and LO
simulations are 982 cm^{-3}, 1027 cm^{-3}, 1057 cm^{-3}, respectively, but the observation was 2154 cm^{-3}. Such underestimated CCN
concentrations seem to be due to the systematic error in WRF-Chem. As discussed in Tuccella et al. (2015), the uncertainty of
updraft velocity parameterization and bulk hygroscopicity of aerosols lead to underestimation of CCN concentration and CCN
efficiency (CCN/CN) by a factor of 1.5 and 3.8, respectively. Nevertheless, over land, AS, RA and LO simulate similar values
of f_{CCN} because continental sulfate aerosols are generally expected to be fully neutralized form of sulfate [i.e. $(NH_4)_2SO_4$]. This
was not the case over sea. During KORUS-AQ, the aircraft passed over the Yellow Sea on 22 and 25 May 2016 (blue shades
in Fig. 4). For this occasion, LO simulates the highest f_{CCN} over the sea among all simulations because LO uses the prescribed
κ_{SO_4} value of $\kappa_{H_2SO_4}$ over sea. RA simulates slightly lower f_{CCN} over the sea because transportation of continental pollutants
over the sea can be taken into account, as observed during the KORUS-AQ campaign. The transported air pollutants increase
the ammonium concentration over the sea, neutralize H_2SO_4, reduce the hygroscopicity of sulfate aerosols, and consequently
decrease f_{CCN}. Simulated f_{CCN} in RA has a high spatiotemporal correlation with the observation over the Yellow Sea (i.e., 0.83),
while AS shows a rather lower correlation (i.e., 0.65). Such difference stems from the fact that R value vary significantly over
the Yellow sea due to the transportation of anthropogenic chemicals by westerlies and such variability is taken into account in
RA. This improvement highlights the importance of appropriate chemical representation in atmospheric models. Compared to
the RA and LO simulations, AS predicts the lowest f_{CCN} because the lowest κ_{SO_4} ($=\kappa_{(NH_4)_2SO_4}$) is prescribed over sea as well
as over land.

We conducted a reliability test that has been often used to evaluate the performance of air quality models. Kumar et
al. (1993) proposed the following three criteria for judging model reliability: 1) the normalized mean squared error (NMSE)
below 0.5; 2) the fractional bias ($= 2 \times \frac{\overline{obs} - \overline{sim}}{\overline{obs} + \overline{sim}}$, obs indicates the observed values, sim indicates the simulated values, and the
bar above the symbols indicate the average) between -0.5 and 0.5; and 3) the ratio of the model values to the observed values
($= sim/obs$) between 0.5 and 2.0. These values for AS, RA and LO are compared in Table 3. It indicates that RA and LO
satisfy all three criteria but AS does not satisfy two of the three criteria as it predicts a rather high normalized NMSE and

fractional bias. Between RA and LO, LO seems somewhat closer to observation than RA but the difference is small for these calculations.

The variation of κ_{SO_4} almost directly influences the change in column-integrated f_{CCN} (Fig. 5). RA predicts higher f_{CCN} than AS over the coastal land regions because the occasionally very low ammonium concentration lowers R and affects

245   the CCN activation. Meanwhile, SA prescribes κ_{SO_4} value two times as high as AS does and produces about 20% higher f_{CCN}.

4.4 Cloud microphysical properties

Different κ_{SO_4} parameterizations affect simulated cloud microphysical properties. Figure 6 shows the relative differences of the simulated column-integrated cloud droplet number concentration (CDNC) in RA, LO, and SA from AS. All three produce higher κ_{SO_4} values than AS, and therefore simulate higher CDNCs. However, the differences in CDNC does not

250   exactly correspond to the differences in f_{CCN} (Fig. 5) because cloud droplet activation is also affected by in-cloud supersaturation and other meteorological factors. SA simulates higher CDNC than AS over both land and sea, but RA and LO simulate higher CDNC mostly only over sea. RA and LO produce similar CDNC distributions over the Yellow Sea (compare Fig. 6a and Fig. 6b) although RA produces smaller f_{CCN} than LO (compare Fig. 5a and Fig. 5b). As in Moore et al. (2011), the reason for that may be because the sensitivity on f_{CCN} reduces so much because supersaturation is so high that most aerosols

255   can act as CCN regardless of their critical supersaturation. That is, the supersaturation over the Yellow Sea is high enough to activate most aerosols to cloud droplets. Over land, RA simulates higher CDNC (up to 12%) than AS in southeast China and the Korean Peninsula, but LO simulates CDNC similar to AS. The results of RA seem to be related to the dilution of ammonium concentrations along the coastal land regions due to the intrusion of maritime air. However, such variation of ammonium cannot be taken into account in LO.

260   Overall, high CDNCs in RA, LO, and SA (Table 1) result in less precipitation but larger LWP, compared to AS (Table 2). Precipitation reduction is more pronounced over sea because of larger relative differences in CDNC. These results agree well with some previous studies; i.e., high CDNCs suppress local precipitations, prolong cloud lifetime, and consequently increase net LWP, which is known as cloud lifetime effect (Albrecht, 1989). Obviously, SA that assumes sulfate aerosols are all H_2SO_4 particles produces the highest CDNC and also the largest differences in all other properties in Table 2.

265   Less rainwater in SA than in any other simulations may also imply that precipitation scavenging of aerosols was less efficient and therefore retaining more aerosols (CCN) to produce more cloud drops and longer cloud lifetime. On average, SA has 103 cm^{-3} more aerosols over sea and 116 cm^{-3} more aerosols over land than LO. These surplus aerosols certainly have potential to simulate higher number of CCN in SA than LO.

For the same LWP condition, high CDNC induces small effective radii (r_e). RA, LO, and SA simulate smaller r_e than

270   AS and the maximum difference of r_e amounts to be 1.46 μm, 1.38 μm, and 1.48 μm, respectively. However, the domain averaged differences of r_e are not as substantial as the differences of other cloud microphysical properties (Table 2). This may be related to somewhat larger LWPs in RA, LO and SA than AS and the sufficient water supply during droplet growth. All

simulations in this study have high water vapor path (WVP) conditions (WVP> 30 kg m^{-2}) throughout the whole domain. According to Qiu et al. (2017), cloud droplets have small competition for water vapor and high chance of collision-coalescence

275 under high WVP conditions (i.e., WVP>1.5 cm or 15 kg m^{-2}). If LWP is similar, r_e difference could be larger among the simulations than that are shown herein.

4.5 Cloud radiative effects

Cloud microphysical properties determine cloud optical properties and therefore control the cloud radiative effects. For a fixed LWP, high CDNC is usually associated with small r_e but large cloud optical thickness. Then optically thick clouds

280 reflect more sunlight and strengthen cloud radiative cooling effect at the top of the atmosphere (TOA), which is known as cloud albedo effect (Twomey, 1974). We calculate the cloud radiative effect at the TOA (CRE) by subtracting the clear sky downward radiation from the net all-sky downward radiation (including clouds) (Hartmann, 2015).

RA, LO, and SA simulate optically thicker clouds that reflect more sunlight and exert stronger cooling effects at the TOA than AS (Fig. 7). For the domain average, the differences of CRE for RA, LO, and SA from AS amount to be about -1.7,

285 -1.5, and -2.1 W m^{-2}, respectively. These differences are most pronounced over sea (Figs. 7b, 7c and 7d). Such pronounced difference over sea may be affected by large cloud fraction around the East China Sea due to the East Asian Summer Monsoon (Pan et al., 2015). That is, large cloud fraction exerts large CRE cooling, so the impact of the new parameterization of κ_{SO_4} on CRE could be substantial under large cloud fraction condition. Note that in the latitude band of 25-28 °N, CRE is similar over the land and over the sea in AS (Fig. 7a) but the CRE differences between RA, LO and SA, and AS are much higher over the

290 sea than over the land (Fig. 7b, 7c and 7d). Such enhanced cooling effect over sea can be explained by increases in CDNC (Fig. 6) and somewhat by increases in LWP (Table 2). According to some previous studies, the contribution of CDNC and LWP to CRE could be larger than 56% (Sengupta et al., 2003; Goren and Rosenfeld, 2014).

5 Summary and conclusions

295 This study introduced a new hygroscopicity parameterization method of sulfate aerosols in the WRF-Chem model and demonstrates the impacts of different κ_{SO_4} parameterization on simulating cloud microphysical properties in East Asia. The new κ_{SO_4} parameterization considered the composition effect of H$_2$SO$_4$ and (NH$_4$)$_2$SO$_4$, using the molar ratio of ammonium to sulfate, R. We also suggest an alternative κ_{SO_4} parameterization: $\kappa_{(NH_4)_2SO_4}$ for land and $\kappa_{H_2SO_4}$ for sea, which utilizes the information of the typical observed geographical distribution of sulfate aerosols, in case when ammonium data are

300 not available. The performance of the new κ_{SO_4} parameterizations was evaluated by comparing with observational data obtained from a field campaign in East Asia and it was demonstrated that the new κ_{SO_4} parameterizations could produce more reliable aerosol and CCN concentrations than the previous method that uses a single κ_{SO_4} (i.e., $\kappa_{(NH_4)_2SO_4}$). To note is that the

The effect of the new κ_{SO_4} parameterizations is indicated as substantially different cloud microphysical properties especially over the sea (about 20% increases in CDNC). The increases of CDNC suppress local precipitation, prolong cloud lifetime, and consequently reflect more sunlight, i.e., more cooling effect (about 1.5 W m^{-2}) than the simulation with the original κ_{SO_4} parameterization in WRF-Chem that assumes $\kappa_{SO_4} = \kappa_{(NH_4)_2SO_4}$ for all sulfate aerosols. These results indicate that the estimated cloud radiative forcing due to aerosol–cloud interactions can vary significantly with different κ_{SO_4} parameterizations.

The importance of oceanic sulfate aerosols on radiative forcing is highlighted in recent studies which suggested that DMS (precursor of oceanic sulfate aerosols) emissions significantly contribute to the total radiative forcing due to aerosol–cloud interactions (Carslaw et al., 2013; Yang et al., 2017). The new κ_{SO_4} parameterizations could be more appropriate for studying the effects of oceanic sulfate aerosols on climate, compared to other approaches that use a single κ_{SO_4} (i.e., $\kappa_{(NH_4)_2SO_4}$) or use an empirical relationship between (NH₄)₂SO₄ and CCN to calculate CCN activation (Boucher and Anderson, 1995; Kiehl et al., 2000). All in all, the new κ_{SO_4} parameterization is capable of considering the variation of κ_{SO_4} and simulates more reliable results, compared to the previous method using a single κ_{SO_4} value in the calculation of cloud microphysical properties. Many atmospheric models neglect the differences of hygroscopicity between H₂SO₄ and (NH₄)₂SO₄ for simplicity. However, this could result in large uncertainties in estimating CRE, especially in East Asia, as demonstrated in our results.

Therefore, we propose this new parameterization of κ_{SO_4} that considers both of the two dominant sulfate aerosols, H₂SO₄ and (NH₄)₂SO₄, for investigating the effects of sulfate aerosols on climate, especially for East Asia, which shows distinctly different emission patterns over land and sea. The new parameterizations are applicable to calculate CCN activation without additional treatments of the chemical reactions and computational expenses. The new parameterization introduced in this study is expected to work effectively in the domain where land and sea are almost evenly distributed, or in the regions with varying distribution of ammonium to sulfate molar ratio. However, we tested the performance of the new κ_{SO_4} parameterization only in East Asia due to the limited amount of observation data available to validate the performance of CCN activation. Therefore, further studies are needed for different regions where observation data are available to confirm the reliability of our new parameterization.

that different treatment of sulfate aerosols did not significantly affect nitrate and sea salt aerosols. However, it is difficult to estimate how the presence of nitrate and sea salt aerosols impacted the results in our simulations. Future study may need to address such important issue in more detail.

Code availability

340   The original WRF-Chem v3.8.1 source code is available at https://www2.mmm.ucar.edu/wrf/users/download/get_sources.html (Grell et al., 2005; Fast et al., 2006; Skamarock et al., 2008; Peckham et al., 2011). The optimized sulfate aerosol hygroscopicity parameter code is available at https://zenodo.org/record/3899838#.Xusv82ozZTY; DOI: 10.5281/zenodo.3899838.

Data availability

345   The National Center for Environment Prediction–Climate Forecast System Reanalysis (NCEP–CFSR) data for initial and boundary conditions are obtained from https://rda.ucar.edu/datasets/ds093.1/ (Saha et al., 2014). Anthropogenic emission inventories are obtained from Emissions Database for Global Atmospheric Research–Hemispheric Transport of Air Pollution (EDGAR–HTAP; Janssens-Maenhout et al., 2015). The data measured from DC-8 aircraft during the KORUS–AQ campaign is available at https://www-air.larc.nasa.gov/missions/korus-aq/.

350 **Author contributions.**

     AK constructed the idea, designed the optimization method and wrote the first draft of the manuscript. SSY acquired funding and supervised the whole study, and edited the manuscript. DYC participated in the construction of the idea and development of the optimization method, and edited the manuscript. MP provided the KORUS-AQ Champaign data and edited the manuscript.

355 **Acknowledgement**

This work was funded by the Korea Meteorological Administration Research and Development Program under Grant KMI2018-03511.

Reference

Abdul-Razzak, H., Ghan, S. J. and Rivera-Carpio, C.: A parameterization of aerosol activation. Part I: Single aerosol type, J.
360   Geophys. Res., 103, 6123–6131, doi:10.1029/97jd03735, 1998.

Abdul-Razzak, H. and Ghan, S. J.: A parameterization of aerosol activation: 2. Multiple aerosol types. J. Geophys. Res., 105, 6837–6844, doi:10.1029/1999jd901161,2000.

Ackermann, I.J., Hass, H., Memmesheimer, M., Ebel, A., Binkowski, F.S., and Shankar U.: Modal aerosol dynamics model for Europe: Development and first applications, Atmos. Env., 32(17), 2981–2999, doi:10.1016/s1352-2310(98)00006-5,1998.

365   Albrecht, B. A.: Aerosols, cloud microphysics and fractional cloudiness, Science, 245, 1227–1230, doi:10.1126/science.245.4923.1227, 1989.

Al-Saadi, J., Carmichael, G., Crawford, J., Emmons, L., Song, C. K., Chang, L. S., Lee, G., Kim, J., and Park, R., 2015. NASA contributions to KORUS-AQ: An international cooperative air quality field study in Korea. NASA White Pap., https//goo.gl/VhssdX, 2016.

370   Aneja V. P.: Natural sulfur emissions into the atmosphere. J. Air Waste Manage Assoc., 40(4), 469–476, doi:10.1080/10473289.1990.10466701, 1990.

Baró, R., Jiménez-Guerrero, P., Balzarini, A., Curci, G., Forkel, R., Grell, G., Hirtl, M., Honzak, L., Langer, M., Pérez, J. L., Pirovano, G., San José, R., Tuccella, P., Werhahn, J., Žabkar, R.: Sensitivity analysis of the microphysics scheme in WRF-Chem contributions to AQMEII phase 2, Atmos. Env., 115, 620–629, doi:10.1016/j.atmosenv.2015.01.047, 2015.

375   Bessagnet, B., Pirovano, G., Mircea, M., Cuvelier, C., Aulinger, A., Calori, G., Ciarelli, G., Manders, A., Stern, R., Tsyro, S., García Vivanco, M., Thunis, P., Pay, M.-T., Colette, A., Couvidat, F., Meleux, F., Rouïl, L., Ung, A., Aksoyoglu, S., Baldasano, J. M., Bieser, J., Briganti, G., Cappelletti, A., D'Isidoro, M., Finardi, S., Kranenburg, R., Silibello, C., Carnevale, C., Aas, W., Dupont, J.-C., Fagerli, H., Gonzalez, L., Menut, L., Prévôt, A. S. H., Roberts, P., and White, L.: Presentation of the EURODELTA III intercomparison exercise – evaluation of the chemistry transport models' performance on criteria

380   pollutants and joint analysis with meteorology, Atmos. Chem. Phys., 16, 12667–12701, doi:10.5194/acp-16-12667-2016, 2016.

Bishop, G. A. and Stedman, D. H.: Reactive Nitrogen Species Emission Trends in Three Light-/Medium-Duty United States Fleets. Environ. Sci. Technol., 49(18), 11234−11240, doi:10.1021/acs.est.5b02392, 2015.

Boucher, O., and Anderson, T. L.: General circulation model assessment of the sensitivity of direct climate forcing by

385   anthropogenic sulfate aerosols to aerosol size and chemistry, J. Geophys. Res., 100(D12), 26117– 26134, doi:10.1029/95JD02531, 1995.

Boucher, O., Randall, D., Artaxo, P., Bretherton, C., Feingold, G., Forster, P. , Kerminen, V.-M., Kondo, Y., Liao, H., Lohmann, U., Rasch, P., Satheesh, S.K., Sherwood, S. , Stevens, B., and Zhang, X.Y.: Clouds and Aerosols. In: Climate Change 2013: The Physical Science Basis. Contribution of Working Group I to the Fifth Assessment Report of the

390   Intergovernmental Panel on Climate Change [Stocker, T.F., Qin, D., Plattner, G.-K., Tignor, M., Allen, S.K., Boschung, J., Nauels, A., Xia, Y., Bex, V., and Midgley, P.M. (eds.)]. Cambridge University Press, Cambridge, United Kingdom and New York, NY, USA, 2013.

Carslaw, K.S., Lee, L.A., Reddington, C.L., Pringle, K.J., Rap, A., Forster, P.M., Mann, G.W., Spracklen, D.V., Woodhouse, M.T., Regayre, L.A., and Pierce, J. R.: Large contribution of natural aerosols to uncertainty in indirect forcing, Nature, 503,

395   67–71, doi:10.1038/nature12674, 2013.

Ceburnis, D., Rinaldi, M., Ovadnevaite, J., Martucci, G., Giulianelli, L., and O'Dowd, C. D.: Marine submicron aerosol gradients, sources and sinks, Atmos. Chem. Phys., 16, 12425–12439, doi:10.5194/acp-16-12425-2016, 2016.

Chang, D., J. Lelieveld, H. Tost, B. Steil, A. Pozzer, and J. Yoon: Aerosol physicochemical effects on CCN activation simulated with the chemistry-climate model EMAC, Atmos. Environ., 162, 127–140, doi:10.1016/j.atmosenv.2017.03.036,

400   2017.

Chang, J.S., Binkowski, F.S., Seaman, N.L., McHenry, J.N., Samson, P.J., Stockwell, W.R., Walcek, C.J., Madronich, S., Middleton, P.B., Pleim, J.E., and Lansford, H.H.: The regional acid deposition model and engineering model. State-of-Science/Technology, Report 4, National Acid Precipitation Assessment Program, Washington, DC, 1989.

Chapman, E. G., Gustafson Jr., W. I., Easter, R. C., Barnard, J. C., Ghan, S. J., Pekour, M. S., and Fast, J. D.: Coupling aerosol-

405   cloud-radiative processes in the WRF-Chem model: Investigating the radiative impact of elevated point sources, Atmos. Chem. Phys., 9, 945-964, doi:10.5194/acp-9-945-2009, 2009.

Charlson, Robert J., Wigley, Tom M. L., Sulfate Aerosol and Climatic Change, Scientific American, 270(2), 48–57, doi:10.1038/scientificamerican0294-48, 1994.

Chen, J., Zhao, C. S., Ma, N., and Yan, P.: Aerosol hygroscopicity parameter derived from the light scattering enhancement

410   factor measurements in the North China Plain, Atmos. Chem. Phys., 14, 8105–8118, doi:10.5194/acp-14-8105-2014, 2014.

Clegg, S. L., Brimblecombe, P., andWexler, A. S.: Thermodynamic model of the system H^+–NH_4^+–Na^+–SO_4^{2-}–NH_3–Cl^-–H_2O at 298.15 K, J. Phys. Chem. A., 102(12), 2155–2171, doi:10.1021/jp973043j, 1998.

Dibb, J. E., Talbot, R. W., Scheuer, E. M., Seid, G., Avery, M. A., and Singh, H. B.: Aerosol chemical composition in Asian continental outflow during the TRACE-P campaign: Comparison with PEM-West B, J. Geophys. Res., 108(D21), 8815,

415   doi:10.1029/2002JD003111, 2003.

Dusek, U., Frank, G. P., Hildebrandt, L., Curtius, J., Schneider, J., Walter, S., Chand, D., Drewnick, F., Hings, S., Jung, D., Borrmann, S., and Andreae, M. O.: Size matters more than chemistry for cloud nucleating ability of aerosol particles, Science, 312, 1375–1378, doi:10.1126/science.1125261, 2006.

Elleman, R. A., and Covert, D. S.: Aerosol size distribution modeling with the Community Multiscale Air Quality modeling

420   system in the Pacific Northwest: 2. Parameterizations for ternary nucleation and nucleation mode processes, J. Geophys. Res., 114(D11207), doi:10.1029/2009JD012187, 2009.

Fast J.D , Gustafson W.I Jr, Easter R.C , Zaveri R.A , Barnard J.C , Chapman E.G. , Grell G.A.: Evolution of ozone, particulates, and aerosol direct forcing in an urban area using a new fully coupled meteorology, chemistry, and aerosol model, J. Geophys. Res., 111, D21305, doi:10.1029/2005jd006721, 2006.

425   Fisher, J. A., Jacob, D. J., Wang, Q., Bahreini, R., Carouge, C. C., Cubison, M. J., Dibb, J. E., Diehl, T., Jimenez, J. L., Leibensperger, E. M., Lu, Z., Meinders, M. B. J., Pye, H. O. T., Quinn, P. K., Sharma, S., Streets, D. G., van Donkelaar, A.,

and Yantosca, R. M.: Sources, distribution, and acidity of sulfate–ammonium aerosol in the Arctic in winter–spring, Atmos. Env., 45(39), 7301–7318, doi:10.1016/j.atmosenv.2011.08.030, 2011.

Fountoukis, C., and Nenes, A.: Continued development of a cloud droplet formation parameterization for global climate
430 models, J. Geophys. Res., 110, D11212, doi:10.1029/2004JD005591., 2005.

Fujita, S.-I., Takahashi, A., Weng, J.-H., Huang, L.-F., Kim, H.-K., Li, C.-K., Huang, F. T. C., and Jeng, F.-T.: Precipitation chemistry in East Asia, Atmos. Env., 34(4), 525–537, doi:10.1016/S1352-2310(99)00261-7, 2000.

Gasteiger, J. and Wiegner, M.: MOPSMAP v1.0: a versatile tool for the modeling of aerosol optical properties, Geosci. Model Dev., 11, 2739–2762, doi:10.5194/gmd-11-2739-2018, 2018.

435 Georgiou, G. K., Christoudias, T., Proestos, Y., Kushta, J., Hadjinicolaou, P., and Lelieveld, J.: Air quality modelling in the summer over the eastern Mediterranean using WRF-Chem: chemistry and aerosol mechanism intercomparison, Atmos. Chem. Phys., 18, 1555–1571, doi:10.5194/acp-18-1555-2018, 2018.

Ghan, S. J., Abdul-Razzak, H., Nenes, A., Ming, Y., Liu, X., Ovchinnikov, M., Shipway, B., Meskhidze, N., Xu, J., and Shi, X.: Droplet nucleation: Physically-based parameterizations and comparative evaluation, J. Adv. Model. Earth Syst., 3,
440 M10001, doi:10.1029/2011MS000074, 2011.

Good, N., Topping, D. O., Allan, J. D., Flynn, M., Fuentes, E., Irwin, M., Williams, P. I., Coe, H., and McFiggans, G.: Consistency between parameterisations of aerosol hygroscopicity and CCN activity during the RHaMBLe discovery cruise, Atmos. Chem. Phys., 10, 3189–3203, doi:10.5194/acp-10-3189-2010, 2010.

Goren, T., and Rosenfeld, D.: Decomposing aerosol cloud radiative effects into cloud cover, liquid water path and Twomey
445 components in marine stratocumulus, Atmos. Res., 138, 378–393, doi:10.1016/j.atmosres.2013.12.008, 2014.

Grell, G. A., and A. Baklanov: Integrated modeling for forecasting weather and air quality: A call for fully coupled approaches, Atmos. Environ., 45, 6845–6851, doi:10.1016/j.atmosenv.2011.01.017, 2011.

Grell, G. A., Knoche, R., Schmitz, R., McKeen, S. A., Frost, G., Skamarock, W. C., and Eder, B.: Fully-coupled "online" chemistry within the WRF model, Atmos. Environ., 39, 6957–6976, doi:10.1016/j.atmosenv.2005.04.027, 2005.

450 Guenther, A., Karl, T., Harley, P., Wiedinmyer, C., Palmer, P. I., and Geron, C.: Estimates of global terrestrial isoprene emissions using MEGAN (Model of Emissions of Gases and Aerosols from Nature), Atmos. Chem. Phys., 6, 3181–3210, doi:10.5194/acp-6-3181-2006, 2006.

Gustafson, W. I., Chapman, E. G., Ghan, S. J., Easter, R. C., and Fast, J. D.: Impact on modeled cloud characteristics due to simplified treatment of uniform cloud condensation nuclei during NEAQS 2004, Geophys. Res. Lett., 34, L19809,
455 doi:10.1029/2007GL030021, 2007.

Hartmann DL (2nd Eds.): Global physical climatology, Elsevier Science, 485 pp., 2016.

Hong, S.–Y., Noh, Y., and Dudhia, J.: A new vertical diffusion package with an explicit treatment of entrainment processes, Mon. Wea. Rev., 134, 2318–2341, doi:10.1175/MWR3199.1, 2006.

Iacono, M. J., Delamere, J. S., Mlawer, E. J., Shephard, M. W., Clough, S. A., and Collins, W. D.: Radiative forcing by long–lived greenhouse gases: Calculations with the AER radiative transfer models, J. Geophys. Res., 113, D13103, doi:10.1029/2008JD009944, 2008.

Im, U., Bianconi, R., Solazzo, E., Kioutsioukis, I., Badia, A., Balzarini, A., Baro, R., Bellasio, R., Brunner, D., Chemel, C., Curci, G., Denier van der Gon, H., Flemming, J., Forkel, R., Giordano, L., Jimenez-Guerrero, P., Hirtl, M., Hodzic, A., Honzak, L., Jorba, O., Knote, C., Makar, P. A., Manders-Groot, A., Neal, L., Perez, J. L., Pirovano, G., Pouliot, G., San Jose, R., Savage, N., Schroder, W., Sokhi, R. S., Syrakov, D., Torian, A., Tuccella, P., Wang, K., Werhahn, J., Wolke, R., Zabkar, R., Zhang, Y., Zhang, J., Hogrefe, C., and Galmarini, S.: Evaluation of operational online-coupled regional air quality models over Europe and North America in the context of AQMEII phase 2. Part II: Particulate Matter, Atmos. Environ., 115, 421–441, doi:10.1016/j.atmosenv.2014.08.072, 2015.

Janssens-Maenhout, G., Crippa, M., Guizzardi, D., Dentener, F., Muntean, M., Pouliot, G., Keating, T., Zhang, Q., Kurokawa, J., Wankmüller, R., Denier van der Gon, H., Kuenen, J. J. P., Klimont, Z., Frost, G., Darras, S., Koffi, B., and Li, M.: HTAP_v2.2: a mosaic of regional and global emission grid maps for 2008 and 2010 to study hemispheric transport of air pollution, Atmos. Chem. Phys., 15, 11411–11432, doi:10.5194/acp-15-11411-2015, 2015.

Jardine K, Yañez-Serrano, A. M., Williams, J., Kunert, N., Jardine, A., Taylor T., Abrell, L., Artaxo, P., Guenther, A., Hewitt, C. N., House, E., Florentino, A. P., Manzi, A., Higuchi, N., Kesselmeier, J., Behrendt, T., Veres, P. R., Derstroff, B., Fuentes, J. D., Martin, S. T., Andreae, M. O.: Dimethylsulfide in the Amazon rainforest, Global Biogeochem. Cycles, 29(1), 19–32, doi:10.1002/2014GB004969, 2015.

Kang, Y., Liu, M., Song, Y., Huang, X., Yao, H., Cai, X., Zhang, H., Kang, L., Liu, X., Yan, X., He, H., Zhang, Q., Shao, M., and Zhu, T.: High-resolution ammonia emissions inventories in China from 1980 to 2012, Atmos. Chem. Phys., 16, 2043–2058, doi:10.5194/acp-16-2043-2016, 2016.

Kazil, J. and Lovejoy, E. R.: A semi-analytical method for calculating rates of new sulfate aerosol formation from the gas phase, Atmos. Chem. Phys., 7, 3447-3459, doi:10.5194/acp-7-3447-2007, 2007.

Khvorostyanov, V. I., and Curry, J. A.: Parameterization of cloud drop activation based on analytical asymptotic solutions to the supersaturation equation, J. Atmos. Sci., 66(7), 1905–1925, doi:10.1175/2009JAS2811.1, 2009.

Kiehl, J. T., Schneider, T. L., Rasch, P. J., Barth, M. C., and Wong, J.: Radiative forcing due to sulfate aerosols from simulations with the National Center for Atmospheric Research Community Climate Model, Version 3, J. Geophys. Res., 105(D1), 1441– 1457, doi:10.1029/1999JD900495, 2000.

Köhler, H.: The nucleus in and the growth of hygroscopic droplets, Trans Farad Soc, 32, 1152–1161, doi:10.1039/tf9363201152, 1936.

Korhonen, H., Carslaw, K. S., Spracklen, D. V., Mann, G. W., and Woodhouse, M. T.: Influence of oceanic dimethyl sulfide emissions on cloud condensation nuclei concentrations and seasonality over the remote Southern Hemisphere oceans: A global model study, J. Geophys. Res., 113, D15204, doi:10.1029/2007JD009718, 2008.

Kristjánsson, J. E.: Studies of the aerosol indirect effect from sulfate and black carbon aerosols, J. Geophys. Res., 107(D15), doi:10.1029/2001JD000887, 2002.

Kukkonen, J., Olsson, T., Schultz, D. M., Baklanov, A., Klein, T., Miranda, A. I., Monteiro, A., Hirtl, M., Tarvainen, V., Boy, M., Peuch, V.-H., Poupkou, A., Kioutsioukis, I., Finardi, S., Sofiev, M., Sokhi, R., Lehtinen, K. E. J., Karatzas, K., San José, R., Astitha, M., Kallos, G., Schaap, M., Reimer, E., Jakobs, H., and Eben, K.: A review of operational, regional-scale, chemical weather forecasting models in Europe, Atmos. Chem. Phys., 12, 1–87, doi:10.5194/acp-12-1-2012, 2012.

Kulmala M., Laaksonen, A., and Pirjola, L.: Parameterizations for sulphric acid/water nucleation rates, J. Geophys. Res., 103, 8301–8308, doi:10.1029/97jd03718, 1998.

Kulmala, M., Korhonen, P., Napari, I., Karlsson, A., Berresheim, H., and O'Dowd, C. D.: Aerosol formation during PARFORCE: Ternary nucleation of H2SO4, NH3, and H2O, J. Geophys. Res., 107, 8111, doi:10.1029/2001JD000900, 2002.

Kumar, A., Luo, J., and Bennett, G.: Statistical Evaluation of Lower Flammability Distance (LFD) using Four Hazardous Release Models, Process Safety Progress, 12(1), 11, doi:10.1002/prs.680120103, 1993.

Kurokawa, J., Ohara, T., Morikawa, T., Hanayama, S., Greet, J.-M., Fukui, T., Kawashima, K., and Akimoto, H.: Emissions of air pollutants and greenhouse gases over Asian regions during 2000–2008: regional emission inventory in Asia (REAS) version 2, Atmos. Chem. Phys., 13, 11019–11058, doi:10.5194/acpd-13-10049-2013, 2013.

Lewis, E. R.: An examination of Köhler theory resulting in an accurate expression for the equilibrium radius ratio of a hygroscopic aerosol particle valid up to and including relative humidity 100%, J. Geophys. Res., 113, D03205, doi:10.1029/2007JD008590, 2008.

Liu, J., Mauzerall, D. L., and Horowitz, L. W.: Source-receptor relationships between East Asian sulfur dioxide emissions and Northern Hemisphere sulfate concentrations, Atmos. Chem. Phys., 8, 3721–3733, doi:10.5194/acp-8-3721-2008, 2008.

Liu, T., Wang, X., Deng, W., Zhang, Y., Chu, B., Ding, X., Hu, Q., He, H., and Hao, J.: Role of ammonia in forming secondary aerosols from gasoline vehicle exhaust, Sci. China: Chem., 58 (9), 1377−1384, doi:10.1007/s11426-015-5414-x, 2015.

Liu, L., , Zhang, X., Xu, W., Liu, X., Lu, X., Wang, S., Zhang, W., and Zhao, L.: Ground Ammonia Concentrations over China Derived from Satellite and Atmospheric Transport Modeling, Remote Sens., 9(5), 467, doi:10.3390/rs9050467, 2017.

Mann, G. W., Carslaw, K. S., Spracklen, D. V., Ridley, D. A., Manktelow, P. T., Chipperfield, M. P., Pickering, S. J., and Johnson, C. E.: Description and evaluation of GLOMAP-mode: a modal global aerosol microphysics model for the UKCA composition-climate model, Geosci. Model Dev., 3, 519–551, doi:10.5194/gmd-3-519-2010, 2010.

Moore, R. H., Bahreini, R., Brock, C. A., Froyd, K. D., Cozic, J., Holloway, J. S., Middlebrook, A. M., Murphy, D. M., and Nenes, A.: Hygroscopicity and composition of Alaskan Arctic CCN during April 2008, Atmos. Chem. Phys., 11, 11,807–11, 825, doi:10.5194/acp-11-11807-2011, 2011.

Moore, R. H., Cerully, K., Bahreini, R., Brock, C. A., Middlebrook, A. M., and Nenes, A.: Hygroscopicity and composition of California CCN during summer 2010, J. Geophys. Res., 117, D00V12, doi:10.1029/2011JD017352, 2012.

Morrison, H., G. Thompson, V. Tatarskii: Impact of Cloud Microphysics on the Development of Trailing Stratiform

525 Precipitation in a Simulated Squall Line: Comparison of One– and Two–Moment Schemes. Mon. Wea. Rev., 137, 991–1007, doi:10.1175/2008MWR2556.1, 2009.

Myhre, G., Shindell, D., Bréon, F.-M., Collins, W., Fuglestvedt, J., Huang, J., Koch, D., Lamarque, J.-F., Lee, D., Mendoza, B., Nakajima, T., Robock, A., Stephens, G., Takemura, T., and Zhang, H.: Anthropogenic and natural radiative forcing, in: Clim. Chang. 2013 Phys. Sci. basis. Contrib. Work. Gr. I to fifth Assess. Rep. Intergov. panel Clim. Chang., 659–740,

530 Cambridge University Press, Cambridge, UK and New York, NY, USA, 2013.

Napari, I., Noppel, M., Vehkamaki, H., and Kulmala, M.: Parametrization of ternary nucleation rates for H2SO4-NH3-H2O vapors, J. Geophys. Res., 107, 4381, doi:10.1029/2002JD002132, 2002.

Nenes, A., Charlson, R. J., Facchini, M. C., Kulmala, M., Laaksonen, A., and Seinfeld, J. H.: Can chemical effects on cloud droplet number rival the first indirect effect? Geophys. Res. Lett., 29(17), 1848, doi:10.1029/2002GL015295, 2002.

535 Nenes, A., Pandis, S. N., and Pilinis, C.: ISORROPIA: A new thermodynamic equilibrium model for multiphase multicomponent aerosols, Aquat. Geochem., 4, 123–152, doi:10.1023/A:1009604003981, 1998.

Pan, Z., Gong, W., Mao, F., Li, J., Wang, W., Li, C., and Min, Q.: Macrophysical and optical properties of clouds over East Asia measured by CALIPSO, J. Geophys. Res. Atmos., 120, 11,653–11,668, doi:10.1002/2015JD023735, 2015.

Park, M., Yum, S. S., Kim, N., Anderson, B. E., Beyersdorf, A., and Thornhill, K. L.: On the submicron aerosol distributions

540 and CCN activity in and around the Korean Peninsula measured onboard the NASA DC-8 research aircraft during the KORUS-AQ field campaign, Atmos. Res., 243, 105004, doi:10.1016/j.atmosres.2020.105004, 2020.

Paulot, F., Jacob, D. J., Pinder, R. W., Bash, J. O., Travis, K., and Henze, D. K.: Ammonia emissions in the United States, European Union, and China derived by high-resolution inversion of ammonium wet deposition data: Interpretation with a new agricultural emissions inventory (MASAGE_NH3), J. Geophys. Res. Atmos., 119, 4343−4364, doi:10.1002/2013jd021130,

545 2014.

Paulot, F., Jacob, D. J., Johnson, M. T., Bell, T. G., Baker, A. R., Keene, W. C., Lima, I. D., Doney, S. C., and Stock, C. A.: Global oceanic emission of ammonia: Constraints from seawater and atmospheric observations, Global Biogeochem. Cycles, 29, 1165–1178, doi:10.1002/2015GB005106, 2015.

Peckham, S., Grell, G. A., McKeen, S. A., Barth, M., Pfister, G., Wiedinmyer, C., Fast, J. D., Gustafson, W. I., Zaveri, R.,

550 Easter, R. C., Barnard, J., Chapman, E., Hewson, M., Schmitz, R., Salzmann, M., and Freitas, S.: WRF-Chem Version 3.3 User's Guide. NOAA Technical Memo., 98 pp., 2011.

Petters, M. D. and Kreidenweis, S. M.: A single parameter representation of hygroscopic growth and cloud condensation nucleus activity, Atmos. Chem. Phys., 7, 1961–1971, doi:10.5194/acp-7-1961-2007, 2007.

Pringle, K. J., Tost, H., Pozzer, A., Pöschl, U., and Lelieveld, J.: Global distribution of the effective aerosol hygroscopicity

555 parameter for CCN activation, Atmos. Chem. Phys., 10, 5241–5255, doi:10.5194/acp-10-5241-2010, 2010.

Qiu, Y., Zhao, C., Guo, J., and Li, J.: 8-Year ground-based observational analysis about the seasonal variation of the aerosol-cloud droplet effective radius relationship at SGP site, Atmos. Env., 164, 139–146, doi:10.1016/j.atmosenv.2017.06.002, 2017.

Qu, Y., An, J., He, Y., and Zheng, J.: An overview of emissions of SO_2 and NO_x and the long-range transport of oxidized sulfur and nitrogen pollutants in East Asia, J. Env. Sci., 44, 13–25, doi:10.1016/j.jes.2015.08.028, 2016.

560   Raymond, T. M., and Pandis, S. N.: Formation of cloud droplets by multicomponent organic particles, J. Geophys. Res., 108(D15), 4469, doi:10.1029/2003JD003503, 2003.

Saha, S., Moorthi, S., Wu, X., Wang, J., Nadiga, S., Tripp, P., Behringer, D., Hou, Y., Chuang, H., Iredell, M., Ek, M., Meng, J., Yang, R., Mendez, M. P., van den Dool, H., Zhang, Q., Wang, W., Chen, M., and Becker, E.: The NCEP Climate Forecast System Version 2, J. Climate, 27, 2185–2208, doi:10.1175/JCLI-D-12-00823.1, 2014.

565   Schell B., I.J. Ackermann, H. Hass, F.S. Binkowski, and A. Ebel: Modeling the formation of secondary organic aerosol within a comprehensive air quality model system, J. Geophys. Res., 106, 28275–28293, doi:10.1029/2001jd000384, 2001.

Sengupta, M., Clothiaux, E. E., Ackerman, T. P., Kato, S., and Min, Q.: Importance of Accurate Liquid Water Path for Estimation of Solar Radiation in Warm Boundary Layer Clouds: An Observational Study, J. Climate, 16, 2997–3009, doi:10.1175/1520-0442(2003)016<2997:IOALWP>2.0.CO;2, 2003.

570   Seinfeld, J. H. and Pandis, S. N.: Atmospheric Chemistry and Physics. John Wiley and Sons, 1203 pp., 2006.

Shiraiwa, M., Li, Y., Tsimpidi, A. P., Karydis, V. A., Berkemeier, T., Pandis, S. N., Lelieveld, J., Koop, T., and Pöschl, U.: Global distribution of particle phase state in atmospheric secondary organic aerosols, Nat. commun., 15002, doi:10.1038/ncomms15002, 2017.

Skamarock, W. C., Klemp, J. B., Dudhia, J., Gill, D. O., Barker, D. M., Duda, M. G., Huang, X.-Y., Wang, W., and Powers, 575   J. G.: A description of the advanced research WRF version 3, NCAR Tech. Note NCAR/TN-475+STR, 113 pp., 2008.

Stier, P., Feichter, J., Kloster, S., Vignati, E., and Wilson, J.: Emission-Induced Nonlinearities in the Global Aerosol System: Results from the ECHAM5-HAM Aerosol-Climate Model, J. Climate, 19(16), 3845–3862, doi:10.1175/jcli3772.1, 2006.

Stritzke, F., Diemel, O., Wagner, S.: TDLAS-based NH3 mol fraction measurement for exhaust diagnostics during selective catalytic reduction using a fiber-coupled 2.2-μm DFB diode laser, Appl. Phys. B: Lasers Opt., 119 (1), 143−152, 580   doi:10.1007/s00340-015-6073-5, 2015.

Sutton, M. A., Reis, S., Riddick, S. N., Dragosits, U., Nemitz, E., Theobald, M. R., Tang, Y. S., Braban, C. F., Vieno, M., Dore, A. J., Mitchell, R. F., Wanless, S., Daunt, F., Fowler, D., Blackall, T. D., Milford, C., Flechard, C. R., Loubet, B., Massad, R., Cellier, P., Personne, E., Coheur, P. F., Clarisse, L., Van Damme, M., Ngadi, Y., Clerbaux, C., Skjøth, C. A., Geels, C., Hertel, O., Kruit, R. J. W., Pinder, R. W., Bash, J. O., Walker, J. T., Simpson, D., Horváth, L., Misselbrook, T. H., 585   Bleeker, A., Dentener, F., and de Vries, W.: Towards a climate-dependent paradigm of ammonia emission and deposition, Philos. Trans. R. Soc., B, 368(1621), 1−13, doi:10.1098/rstb.2013.0166, 2013.

Tegen, I., Neubauer, D., Ferrachat, S., Siegenthaler-Le Drian, C., Bey, I., Schutgens, N., Stier, P., Watson-Parris, D., Stanelle, T., Schmidt, H., Rast, S., Kokkola, H., Schultz, M., Schroeder, S., Daskalakis, N., Barthel, S., Heinold, B., and Lohmann, U.: The global aerosol–climate model ECHAM6.3–HAM2.3 – Part 1: Aerosol evaluation, Geosci. Model Dev., 12, 1643−1677, 590   doi:10.5194/gmd-12-1643-2019, 2019.

Tewari, M., Chen, F., Wang, W., Dudhia, J., LeMone, M. A., Mitchell, K., Ek, M., Gayno, G., Wegiel, J., and R. H. Cuenca: Implementation and verification of the unified NOAH land surface model in the WRF model. 20th conference on weather analysis and forecasting/16th conference on numerical weather prediction, 11–15 pp. , 2004.

595 Tuccella, P., Curci, G., Grell, G. A., Visconti, G., Crumeyrolle, S., Schwarzenboeck, A., and Mensah, A. A.: A new chemistry option in WRF-Chem v. 3.4 for the simulation of direct and indirect aerosol effects using VBS: evaluation against IMPACT-EUCAARI data, Geosci. Model Dev., 8, 2749–2776, https://doi.org/10.5194/gmd-8-2749-2015, 2015.

Twomey, S.: The nuclei of natural cloud formation: II. The supersaturation in natural clouds and the variation of cloud droplet concentration, Geophys. Pure Appl., 43, 243–249, doi:10.1007/bf01993560, 1959.

Van Damme, M., Clarisse, L., Heald, C. L., Hurtmans, D., Ngadi, Y., Clerbaux, C., Dolman, A. J., Erisman, J. W., and Coheur,
600 P. F.: Global distributions, time series and error characterization of atmospheric ammonia (NH3) from IASI satellite observations, Atmos. Chem. Phys. 14, 2905–2922, doi:10.5194/acp-14-2905-2014, 2014.

VanReken, T. M., Rissman, T. A., Roberts, G. C., Varutbangkul, V., Jonsson, H. H., Flagan, R. C., and Seinfeld, J. H.: Toward aerosol/cloud condensation nuclei (CCN) closure during CRYSTAL-FACE, J. Geophys. Res., 108(D20), 4633, doi:10.1029/2003JD003582, 2003.

605 Waggoner, A. P., Weiss, R. E., and Larson, T. V.: In-situ, rapid response measurement of H2SO4/(NH4)2SO4 aerosols in urban Houston: A comparison with rural Virginia, Atmos. Env., 17(9), 1723–1731, doi:10.1016/0004-6981(83)90179-8, 1967.

Warner, J. X., Dickerson, R. R., Wei, Z., Strow, L. L., Wang, Y., and Liang, Q.: Increased atmospheric ammonia over the world's major agricultural areas detected from space, Geophys. Res. Lett., 44, 2875–2884, doi:10.1002/2016GL072305, 2017.

Watanabe, M., Suzuki, T., O'ishi, R., Komuro, Y., Watanabe, S., Emori, S., Takemura, T., Chikara, M., Ogura, T., Sekiguchi,
610 M., Takata, K., Yamazaki, D., Yokohata, T., Nozawa, T., Hasumi, H., Tatebe, H., and Kimoto, M.: Improved climate simulation by MIROC5: mean states, variability, and climate sensitivity, J. Clim., 23 (23) 6312–6335, doi:10.1175/2010jcli3679.1, 2010.

Wexler, A. S., Lurmann, F. W., and Seinfeld, J. H.: Modelling urban and regional aerosols—I. model development, Atmos. Env., 28(3) 531–546, doi:10.1016/1352-2310(94)90129-5, 1994.

615 Yang, Y., Wang, H., Smith, S. J., Easter, R., Ma, P.-L., Qian, Y., Yu, H., Li, C., and Rasch, P. J.: Global source attribution of sulfate concentration and direct and indirect radiative forcing, Atmos. Chem. Phys., 17, 8903–8922, doi:10.5194/acp-17-8903-2017, 2017.

Zelinka, M. D., Andrews, T., Forster, P. M., and Taylor, K. E.: Quantifying components of aerosol-cloud-radiation interactions in climate models, J. Geophys. Res. Atmos., 119, 7599–7615, doi:10.1002/2014JD021710, 2014.

620 Zhang, K., O'Donnell, D., Kazil, J., Stier, P., Kinne, S., Lohmann, U., Ferrachat, S., Croft, B., Quaas, J., Wan, H., Rast, S., and Feichter, J.: The global aerosol-climate model ECHAM-HAM, version 2: sensitivity to improvements in process representations, Atmos. Chem. Phys., 12, 8911–8949, https://doi.org/10.5194/acp-12-8911-2012, 2012.

Zieger, P., Fierz-Schmidhauser, R., Weingartner, E., and Baltensperger, U.: Effects of relative humidity on aerosol light scattering: results from different European sites, Atmos. Chem. Phys., 13, 10609–10631, doi:10.5194/acp-13-10609-2013, 625   2013.

Tables

Table 1. Domain averaged differences ($= \frac{sensitivity\ simulation - AS}{AS} \times 100\%$) of the CCN activation fraction at 0.6% supersaturation (f_{CCN}) and cloud droplet number concentration (CDNC) in percent. The data are averaged from 0000 UTC 15 May to 0000 UTC 15 June.

	RA–AS		LO–AS		SA–AS	
	Land	Ocean	Land	Ocean	Land	Ocean
f_{CCN} (%)	6	13	1	19	18	22
CDNC (%)	7	20	1	21	14	24

Table 2. Domain averaged water budgets of AS and their differences from other simulations. The data are averaged from 0000 UTC 15 May to 0000 UTC 15 June. Rainwater in this study refers to the liquid phase of water that has a potential of becoming rainfall in the model.

	AS		RA–AS		LO–AS		SA–AS	
	Land	Ocean	Land	Ocean	Land	Ocean	Land	Ocean
Rainwater (g m^{-2})	21.6	39.4	-0.32	-0.60	-0.02	-0.64	-0.52	-0.73
LWP (g m^{-2})	45.7	78.4	0.40	1.41	0.08	1.45	0.73	1.69
IWP (g m^{-2})	9.34	11.2	0.05	0.08	0.02	0.07	0.08	0.09
r_e (μm)	6.13	10.3	-0.02	-0.11	0.00	-0.11	-0.04	-0.12

Table 3. Values of the three criteria suggested in Kumar et al. (1993).

	AS	RA	LO
NMSE < 0.5	0.53	0.48	0.43
-0.5 < Fractional Bias ($= 2 \times \frac{\overline{obs} - \overline{sim}}{\overline{obs} + \overline{sim}}$) < 0.5	0.54	0.50	0.46
0.5 < Ratio ($= sim/obs$) < 2	0.59	0.65	0.65
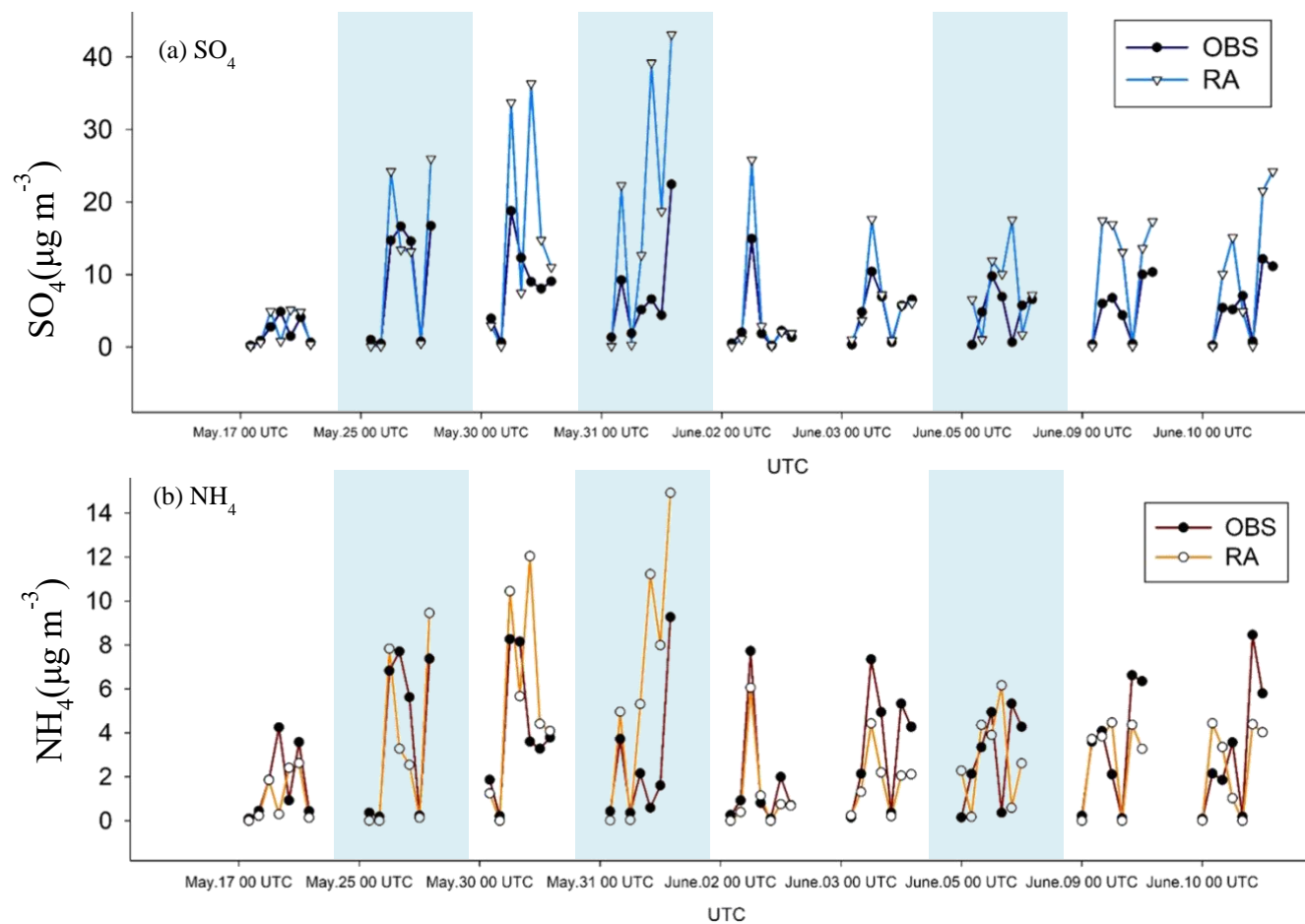
Figure 1. Time variation of the mass concentrations of (a) sulfate and (b) ammonium measured by the NASA DC-8 aircraft (OBS, black line) and simulated by AS (colored line). Blue shaded regions denote the time over the sea.
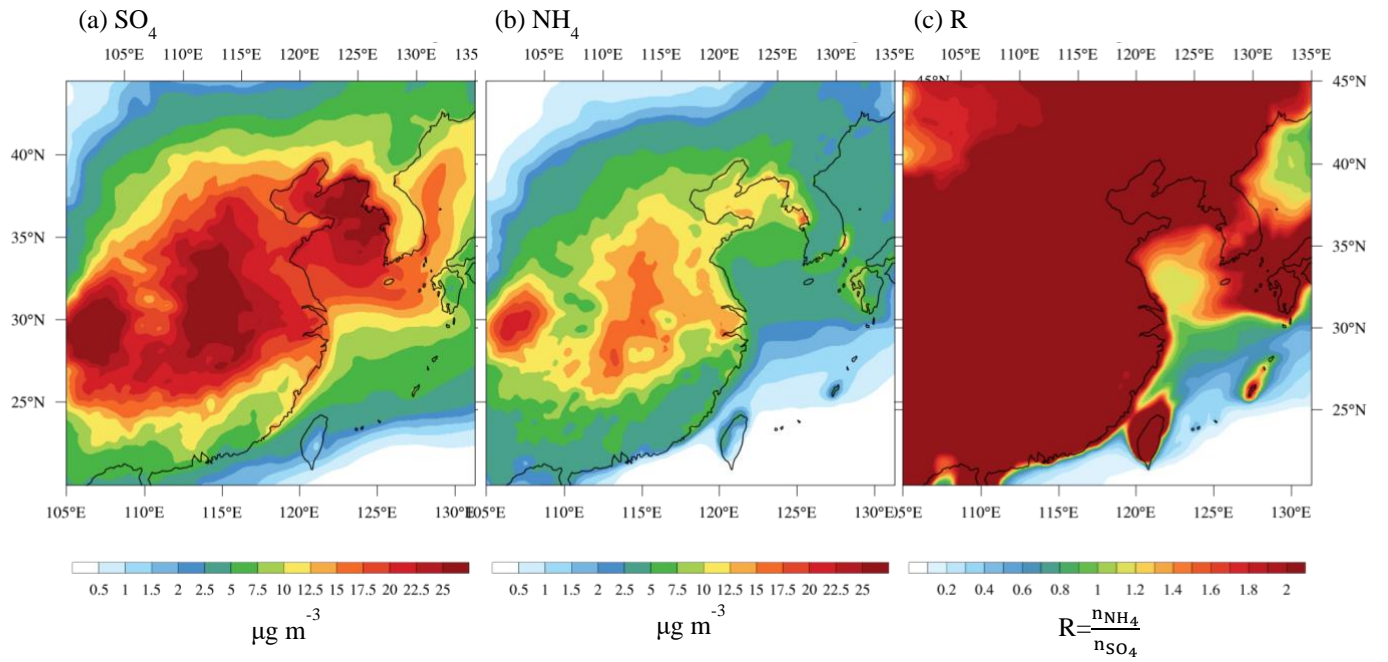
Figure 2. 30 days averaged (0000 UTC 16 May to 0000 UTC 15 June, 2016) spatial distribution of the mass concentrations of (a) sulfate and (b) ammonium, and (c) the molar ratio of ammonium to sulfate (R) at the surface, from AS.
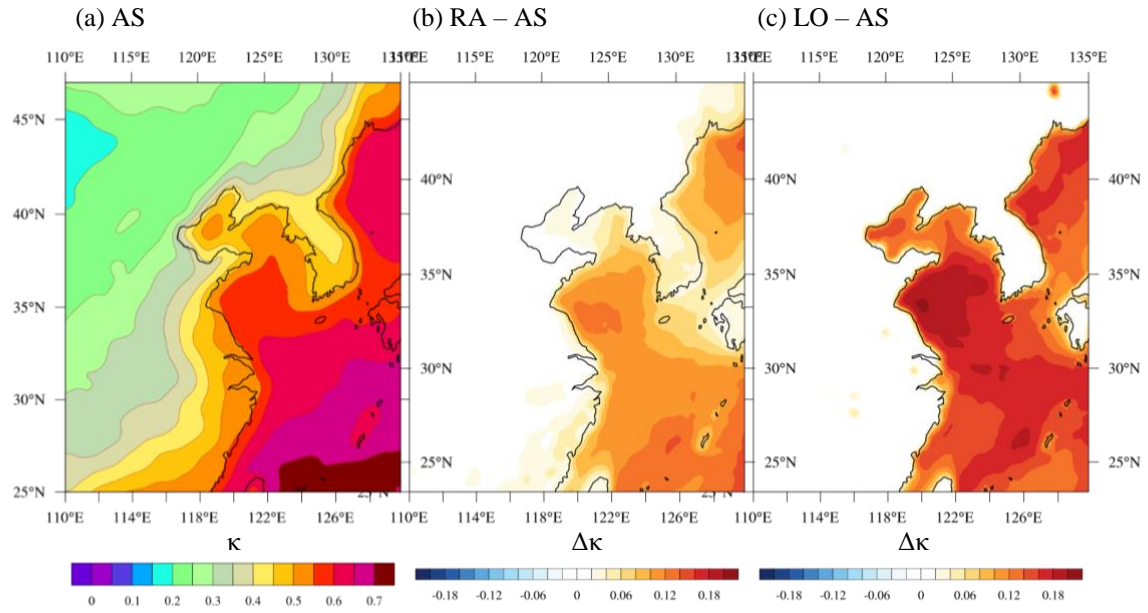
Figure 3. (a) Spatial distribution of the hygroscopicity parameter (κ) at the accumulation mode simulated by AS, the difference of κ (b) between RA and AS, and (c) between LO and AS, at the surface.
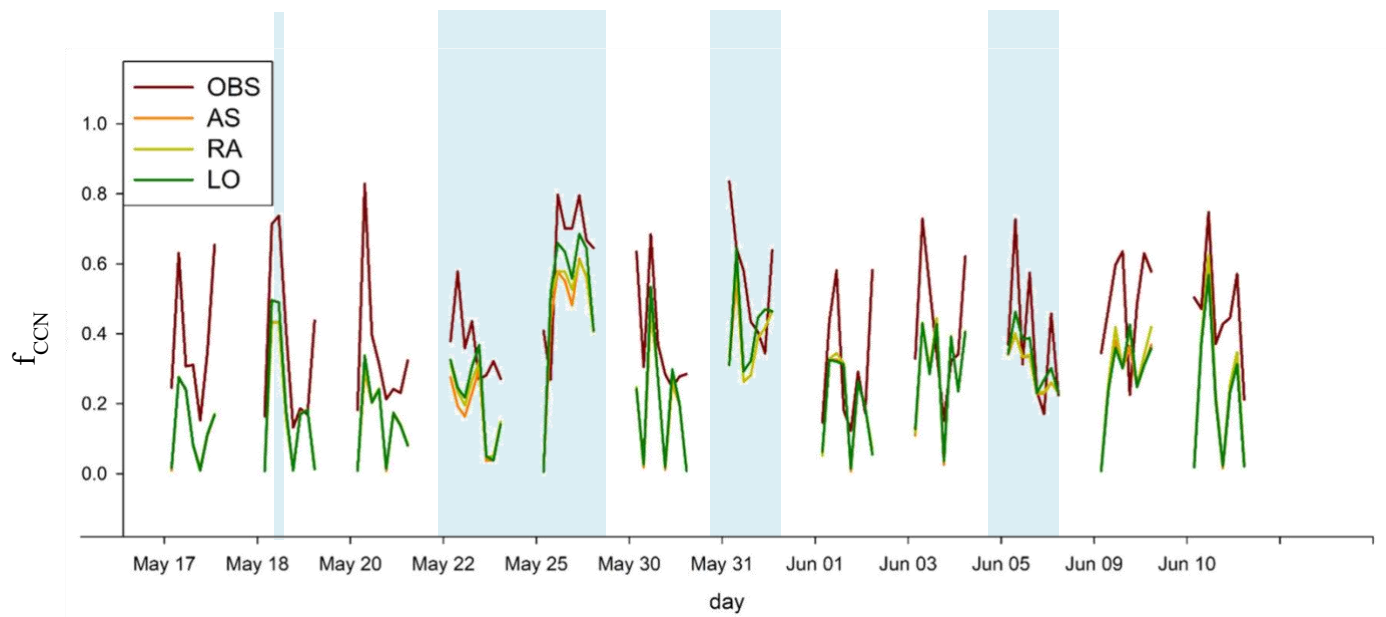
650   **Figure 4**. Time variation of the CCN activation fractions at 0.6% supersaturation (f_{CCN}) measured by the NASA DC-8 aircraft

(OBS) and simulated by AS, RA, and LO. Blue shaded regions denote the time over the sea.
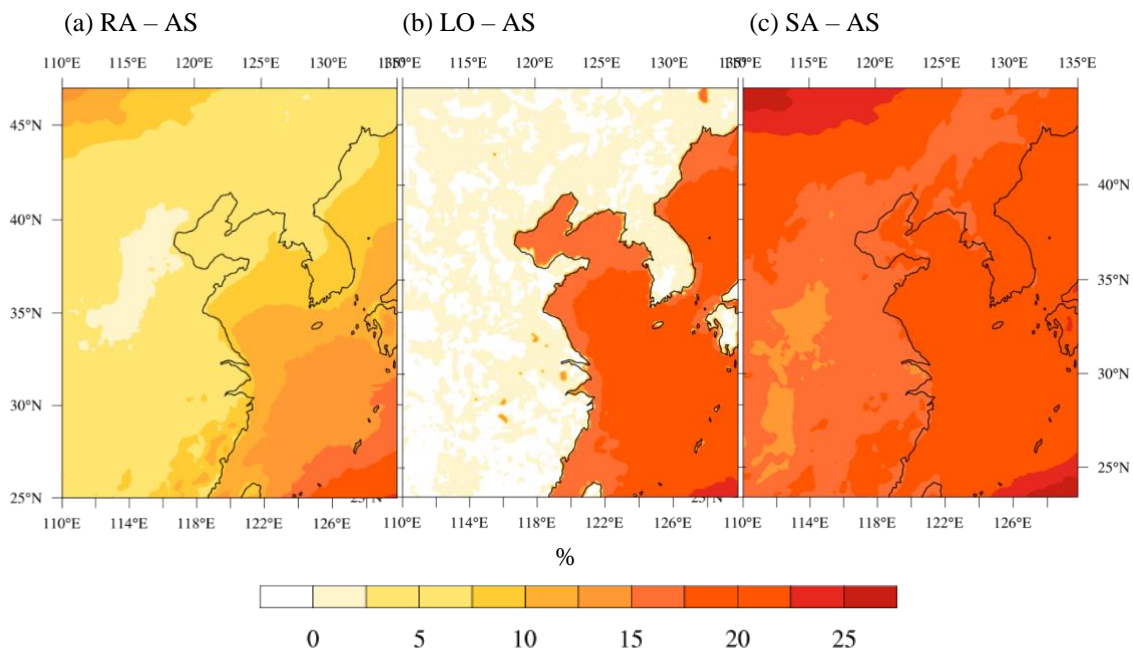
Figure 5. Percentage difference of column-integrated CCN activation fraction at 0.6% supersaturation (f$_{CCN}$) in AS and sensitivity simulations, (a) RA – AS, (b) LO – AS, and (c) SA – AS.

655
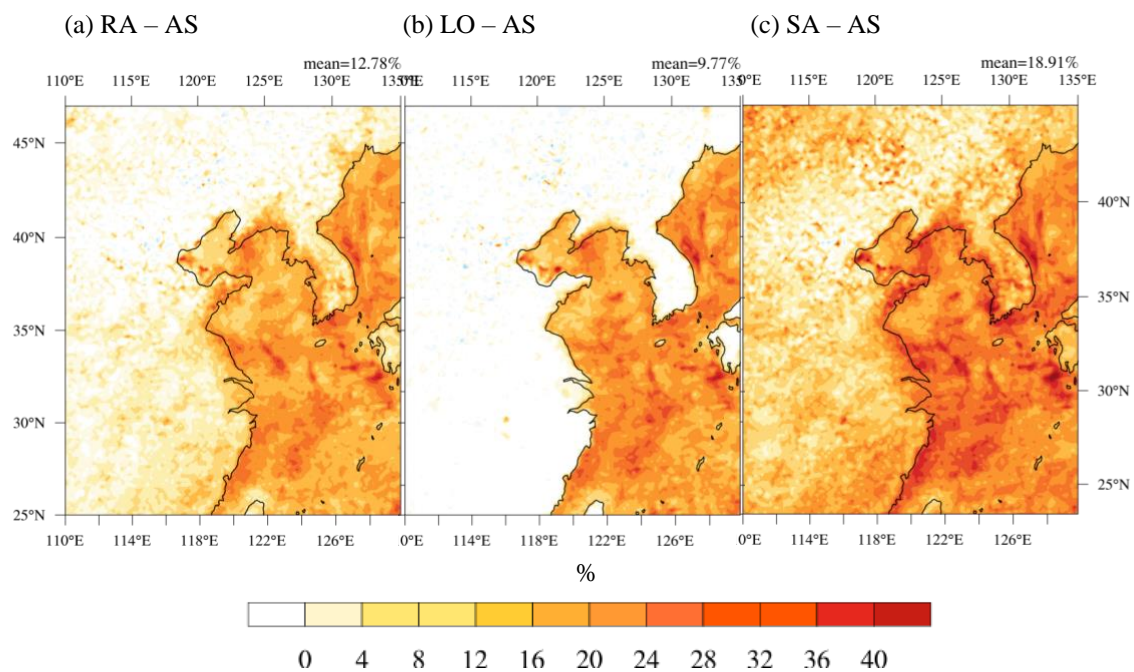
Figure 6. Same as Fig. 5 except for cloud droplet number concentration (CDNC).
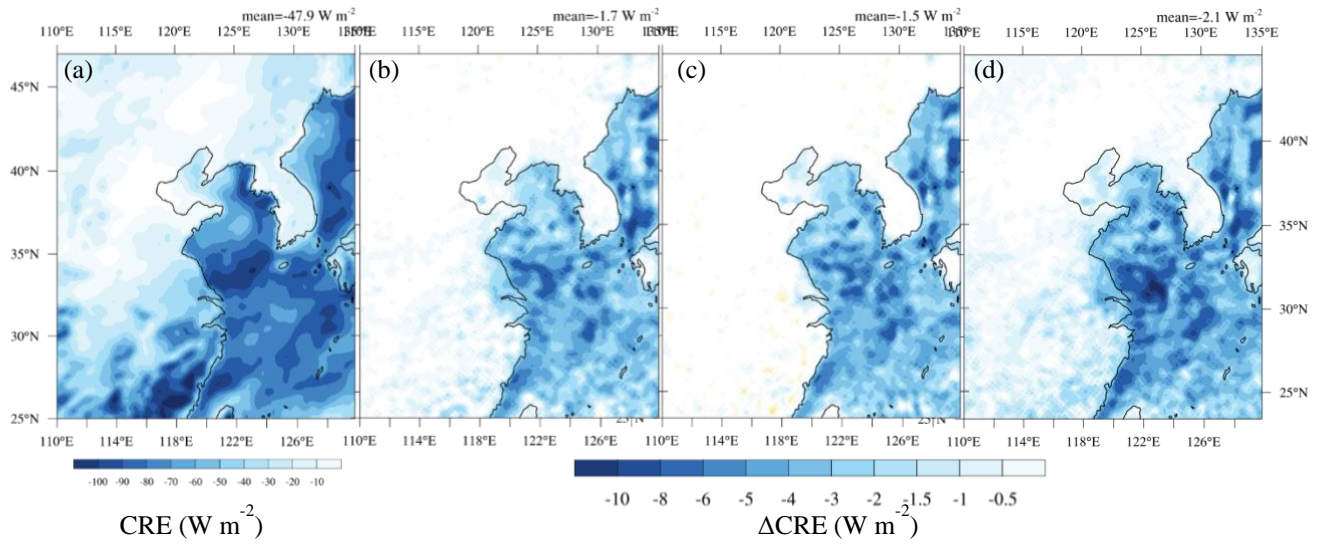
Figure 7. Simulated 30 days averaged (0000 UTC 16 May to 0000 UTC 15 June, 2016) cloud radiative effect (CRE) for (a) AS and the differences (ΔCRE) between (b) RA and AS, (c) LO and AS, and (d) SA and AS.

660